*Journal of Biomedical Materials Research Part B: Applied Biomaterials*

WILEY

Society For Biomaterials

RESEARCH ARTICLE OPEN ACCESS

# Unveiling Bone and Dental Regeneration Potential of Quince Seed Mucilage-Nanohydroxyapatite Scaffolds in Rabbit Mandibles

Cigdem Cetin Genc[1] | Hilal Deniz Yılmaz-Dagdeviren[2] | Yesim Deniz[3] | Burak Derkus[4] | Alpin Degirmenci[1] | Yavuz Emre Arslan[5]

[1]Department of Oral and Maxillofacial Surgery, Faculty of Dentistry, Çanakkale Onsekiz Mart University, Çanakkale, Turkey | [2]Department of Bioengineering, Engineering Faculty, Izmir Institute of Technology, İzmir, Turkey | [3]Department of Oral & Maxillofacial Radiology, Faculty of Dentistry, Çanakkale Onsekiz Mart University, Çanakkale, Turkey | [4]Stem Cell Research Lab., Department of Chemistry, Faculty of Science, Ankara University, Ankara, Turkey | [5]Regenerative Biomaterials Laboratory, Department of Bioengineering, Faculty of Engineering, Çanakkale Onsekiz Mart University, Çanakkale, Turkey

**Correspondence:** Cigdem Cetin Genc (cigdemcetingenc@comu.edu.tr) | Yavuz Emre Arslan (yavuzea@gmail.com)

**Received:** 13 December 2024 | **Revised:** 7 March 2025 | **Accepted:** 16 March 2025

**Funding:** This work was supported by Çanakkale Onsekiz Mart Üniversitesi.

**Keywords:** bone regeneration | critical-size defect | dental regeneration | maxillofacial surgery | nanohydroxyapatite | quince seed mucilage | rabbit

## ABSTRACT

Donor-side morbidity of autografting for maxillofacial region defect regeneration has directed attention to bioengineered scaffolds. Composite scaffolds that mimic the bone extracellular matrix (ECM) are the potential candidates for defect reconstruction. Herein, a plant-based regenerative hydrogel, quince seed mucilage (QSM), was enriched with the nanohydroxyapatite (nHAp) particles to construct composite scaffolds (QSM/nHAp). The emerging scaffold is able to induce cellular spheroid formation and regenerate the critical-sized bilateral mandibular defects in rabbits. The macroscopic observations, histochemical (HC) and immunohistochemical (IHC) stainings, μ-computer tomography (CT) scanning, quantitative real time-polymerase chain reaction (qRT-PCR) analyses, and scanning electron microscopy (SEM) imaging revealed that all QSM/nHAp scaffolds were swelled with host blood, filled the whole cavity, and sustained cellular infiltration without adverse reactions. The gradual biodegradation profile of the scaffolds improved bone regeneration by releasing nHAp particles from the scaffold. Strikingly, co-development of dental and bone regeneration was observed for all QSM/nHAp groups beginning after day 21. Moreover, QSM/nHAp scaffolds induced expression (> 2-fold) of bone and dental-related gene and protein expressions at the grafted area and sustained a proper platform for maxillofacial remodeling. Therefore, we strongly believe that such biocompatible plant-based constructs, compared with conventional medical devices used in maxillofacial surgery, could support and induce simultaneous bone and dental regeneration due to the intrinsic dynamics of the material.

## 1 | Introduction

Maxillofacial region defects due to trauma, tumor formation, infections, and congenital deficiency can cause critical-sized defects characterized by significant bone loss where the natural regeneration process is unattainable [1]. In the clinic, the reconstruction of critical-sized defects is mainly driven by using autologous grafts. The resemblance between autologous grafts and the host tissue significantly reduces the risk of immune rejection and enhances regeneration. However, at least two invasive operations are applied to harvest the autologous graft and reconstruct the defect area. In addition to these

drawbacks, autologous grafts have a natural source limit; upon defect size, the harvested graft for reconstruction can be insufficient to cover the defected region [2]. Currently, bioengineered scaffolds developed for maxillofacial defects have captured interest in preclinical studies to overcome the limitations of regeneration for critical-sized defects. Biocompatible polymers from synthetic or natural origins were utilized as gap filler scaffolds at defective areas in sponge, gel, or woven forms to improve regeneration at the defective side [3, 4]. However, low cellular infiltration, insufficient bioactivity, and impractical design of engineered materials hamper the practical use of most developed materials; therefore, a limited number of newly developed scaffolds can be on stage for clinical practices [4, 5].

Hydroxyapatite is the essential inorganic structure of bone that plays a significant role in the mechanical strength and maturation of bone tissue [6–9]. In the literature, the utilization of hydroxyapatite particles is a very common practice for bone tissue engineering applications due to the bioactivity and biocompatibility of this inorganic mineral [6, 9–12]. On the other hand, the brittle and stiff nature of the hydroxyapatite particles limits their use in bone remodeling applications without combining additional components. Therefore, hydroxyapatite is mostly integrated into a polymer to improve the mechanical toughness and durability of scaffolding material [6, 11–14].

The usage of plant-based materials for tissue engineering applications is becoming popular due to their being pathogen-free, biosafe, biocompatible, green, and economical sources of biopolymers [15–17]. Among them, quince seed mucilage (QSM) extracted from Quince (*Cydonia oblonga*) seeds captured interest nowadays for tissue engineering practices owing to its biological potential. It has wide usage in the traditional medicine of Iranian and East Asian cultures for the treatment of bronchitis, colitis, ulcers, and skin burns [18–21]. In the literature, several in vitro and in vivo experiments were performed with QSM, and its biocompatible and regenerative properties were evaluated for tissue engineering practices [21–27]. Moreover, according to the ISO 10993-3 document, QSM polymer is considered to be biosafe in terms of hemolytic index [18, 28]. Besides, the previous studies published by our group revealed the potential of QSM material for cellular spheroid formation and bone regeneration in vitro [22, 25, 27, 29]. The promising outcomes from this research directed the concerns of QSM polymer for further evaluations at bone remodeling studies in vivo.

Herein, a porous composite scaffold obtained from QSM and nanohydroxyapatite (nHAp) materials was fabricated, and the biological functions of the emerging material in the remodeling of critical-size mandibular defects in rabbit models were evaluated. While the QSM formed the polymeric backbone of the composite scaffolds, providing high water-swelling capacity and a tunable biodegradation profile to guide regenerative effects, nHAp particles enhanced the bone extracellular matrix (ECM) biomimicry and bioactivity [18, 22, 25, 27]. QSM/nHAp was shown to trigger growth-factor-free osteogenic differentiation of human adipose-derived mesenchymal stem cells (MSCs), demonstrating the potential of this composite material in bone tissue regeneration and remodeling [22]. Thus, this study explored the potential of QSM/nHAp scaffolds for bone regeneration in rabbit maxillofacial defects. Critical-size mandibular defects were created bilaterally in 36 male New Zealand rabbits, with scaffolds implanted on one side and the other left blank as a control. Regeneration was evaluated via in-depth analyses. Overall, QSM/nHAp scaffolds demonstrated promising results in efficient bone regeneration, and it is believed that this study contributes a valuable plant-based material for in vivo bone and dental regeneration to the literature.

## 2 | Materials and Methods

### 2.1 | Fabrication of Composite Scaffolds

The extraction method and in-depth characterizations of QSM were presented in our previously published studies [22, 25]. Briefly, a water-based extraction protocol was followed; for that, 4 g of fresh quince seeds were weighed in 75 mL of ultrapure water, and extraction was fulfilled using a rotary evaporator (R-210, Buchi, Switzerland) for 12 h at 30°C. Following the extraction, the QSM was lyophilized (LyoQuest-55, Telstar, Spain) and stored for further usage. The composite solution of QSM and nHAp was prepared at a 1:1 (w/w) ratio using 5 mg/mL QSM and nHAp powder (< 200 nm, 67,741 Sigma-Aldrich). After homogenization with a homogenizer (IKA Turrax T18, Germany), the QSM/nHAp blend was poured into a cylindrical mold (d = 10 mm, $l$ = 4 mm) and then crosslinked with N-(3-dimethylaminopropyl)-N′-ethylcarbodiimide (EDC)-N-hydroxy succinimide (NHS) crosslinkers in ethanol containing (70%) 2-(N-morpholino) ethanesulfonic acid (MES) buffer (pH: 5.5) according to the previously reported protocol [22] (Figure 1). Finally, porous scaffolds were obtained after lyophilization and sterilized under UV light (254 nm) for one hour in a biosafety cabinet.

### 2.2 | Animals and Experimental Design

The experiments were conducted under the approval of the Clinical Research Ethics Committee at "The Faculty of Medicine, Çanakkale Onsekiz Mart University" with a permission number of 2021/05–03. Thirty-six male white New Zealand rabbits, aged five months and weighing 3–3.5 kg, were received and kept ten days in quarantine under veterinary care at Çanakkale Onsekiz Mart University Experimental Research Application and Research Center (ÇOBİLTUM), where all the surgical operations took place. The study was planned according to the Animals in Research: Reporting In Vivo Experiments (ARRIVE) guideline [30, 31]. The sample size was determined via G*Power software (G * Power 3.1, Heinrich Heine University, Germany), t-tests, and the method of the previously reported study elsewhere [32]. The input parameters were set to be the α-type error probability of 0.05, the power 0.85, and the (d) = 0.7318588; the number of subjects was calculated as 69. Since the mandibular defects were created bilaterally, the total number was divided by 2, which yields 35 subjects per group. Due to the experiments being created on the same subject for four different time points (days 10, 21, 45, and 90), one more rabbit was added to have equal subject interruptions. Thus, the total sample number was calculated to be 36 rabbits. For the evaluations, a series of experiments were conducted in the experimental and control groups at four distinct time points. The

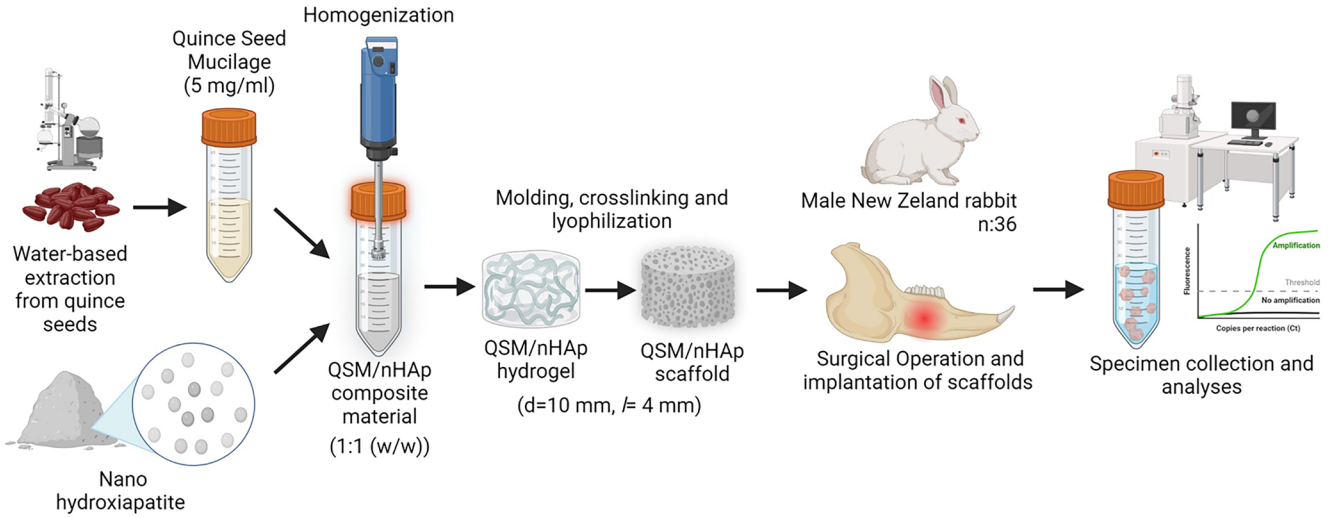


**FIGURE 1** | The representative schematic of QSM/nHAp scaffold production and the summary of the applied protocol for the evaluation of scaffolds in mandibular regeneration in rabbits (created in BioRender.com).

primary endpoint was the assessment of wound healing, osteogenesis, angiogenesis, foreign body reaction, and the outcomes of the early, first intermediate, second intermediate, and late phases. The selected time points were defined as follows: day 10 for evaluating the early-phase inflammatory response within the defect site, day 21 for assessing the initial deposition of bone-like matrix, marking the onset of osteogenic differentiation as reported in the literature, day 45 for monitoring scaffold resorption and bone tissue development during the intermediate phase, and day 90 for analyzing late-stage bone regeneration, matrix maturation, and the biodegradation profile of the scaffold material.

Therefore, after the surgical operation, days 10, 21, 45, and 90 were designated as checkpoints, and a total of 24 rabbits (6 per time point) were used for histological and immunohistochemical (IHC) analyses. Additionally, 4 animals (1 per time point) were allocated for scanning electron microscopy (SEM) evaluation, and 8 animals (2 per time point) were used for quantitative real time-polymerase chain reaction (qRT-PCR) analyses. The randomly assigned rabbits for experimental groups were sacrificed at the time points, and macroscopic evaluations, μ-computer tomography (CT) scanning, histology and immunohistology staining, qRT-PCR, and SEM analysis were performed.

For the surgical operations, all rabbits were anesthetized through intramuscular administration of 35 mg/kg ketamine HCl (Ketalar, Pfizer) and 5 mg/kg XylazineHCl (Rompun, Bayer). Bilateral critical-sized mono cortical mandibular defects, measuring 10 mm × 4 mm in diameter and depth were created on the rabbits' mandibles using a 10 mm trephine bur and physio dispenser. Then, QSM/nHAp scaffolds were implanted on the left side of the mandibula, while the right-side cavity was left empty as a control group. Mini-plate fixation was applied to both sides to prevent further fracture formation. Then, the flap was closed using resorbable suture material, and the rabbits daily received enrofloxacin (Baytril-K, 2.5 mg/kg IM) with meloxicam (Maxicam, 0.2 mg/kg IM) for the following five days after the surgical operation. The subjects were then euthanized on days 10, 21, 45, and 90 with 200 mg/kg (IM) sodium pentothal (Ekipental, Tümekip İlaç Sanayi, Türkiye) injections for further evaluation.

## 2.3 | Macroscopic Evaluations

After the sacrification, specimens were collected using a bur, and the specimens from days 10, 21, 45, and 90 were photographed from a 20 cm distance using a tripod and Canon Eos 6D Mark II camera system (Canon, Japan) to evaluate their macroscopic morphology and fixed using a 10% neutral formalin solution. The Masson's trichrome-stained samples were used for imaging to understand the tissue distribution within samples.

## 2.4 | μ-CT Scanning

The specimens were scanned by the SkyScan 1275 μ-CT (SkyScan, Belgium) system. The radiographic parameters for μ-CT scanning were settled as follows: 65 kVp, 125 mA, 1 mm aluminum filter, 0.02654 mm isotropic voxel size, angular rotation step of 0.2°, 360° scanning, 16-bit pixel depth, 450 projections, and an exposure time of 49 s, resulting in a total scan duration of 29 min. In each sample, the μ-CT sections that exhibited the closest correspondence to the histologic image were carefully chosen and manually aligned with the corresponding images using the histological images as a visual reference. The alignment of μ-CT sections in the coronal, sagittal, and axial planes was carried out using the CTAn software (CTAnalyser; SkyScan) for further investigation.

## 2.5 | Histological Analyses

The collected specimens were fixated in 10% neutral formalin solution, dehydrated, and decalcified for histological evaluations. Then, they were embedded in paraffin and cut into three μm slices. The standard procedure of hematoxylin–eosin (H&E), Masson's trichrome (MT), and Alizarin Red S staining [22, 27] were applied. The IHC staining was also accomplished according to the manufacturer's protocol using primary antibodies of osteopontin (OPN) (1:100, NB110-89062 Novus, USA), osteocalcin (OSC) (1:100, NBP2-89037 Novus, USA) and osteonectin (OSN) (1:100, ab245733 Abcam, UK)

[22]. The mineralization stages and osteogenic development of the specimens were imaged through digital light microscopy (Zeiss, Primostar integrated with Axiocam 105 color camera, Germany), and the histological evaluation of healing was scored [33].

### 2.6 | Quantitative Real-Time PCR Analysis

The expression of osteogenic markers Runx transcription factor 2 (RunX2), alkaline phosphatase (ALP), OPN, and osteoprotegerin (OPG) was evaluated to reveal the osteogenic and dental regeneration process in the mandibular region. For the analyses, specimens were minced into powder via liquid nitrogen, and the total RNA was isolated from tissue specimens via the pureZOL RNA isolation kit (Bio-Rad, USA) according to the manufacturer's manual. After the total RNA isolation, the samples were measured at 260 nm by NanoDrop spectrophotometer to obtain μg/mL value and, from the 1 μg of RNA sample, the cDNA was synthesized by the cDNA kit (iScript, Bio-Rad, USA). Subsequently, the qRT-PCR was performed in triplicate using the master mix and gene-specific primers (Table S1). The related genes were evaluated and expressed as threshold number ($C_t$), normalized against GAPDH as a housekeeping gene. The fold change of each gene was quantified using the $2^{-\Delta\Delta Ct}$ method.

### 2.7 | SEM Imaging

The surface morphology of the specimens was analyzed through SEM (JEOL JSM-7100F, Japan). The collected specimens were fixed with 2.5% glutaraldehyde solution (in PBS), coated with Au/Pt (80:20) for 90 s, and imaged under a 10 kV probe current with various magnifications.

### 2.8 | Statistical Analyses

Statistical analyses for histological examinations were conducted with IBM SPSS for Windows, version 25.0 (SPSS Inc. Chicago, IL, USA). Descriptive statistical values are given as median (max–min). The normality was tested with the Shapiro–Wilk test ($p < 0.05$). Group comparisons were carried out with the Wilcoxon test, intergroup comparisons were analyzed using the Kruskal-Wallis test, and the paired comparisons were performed using the Dunn-Bonferroni test. qRT-PCR statistical analyses were conducted with a minimum of three repetitions, and the results were reported as the standard mean deviation (±). For the experimental data, one-way analysis of variance (ANOVA) analyses followed by Tukey's posthoc tests were performed using Origin Pro software (Origin Lab Corporation, USA). In all tests, the statistical significance was *: $p < 0.05$, **: $p < 0.01$.

## 3 | Results

### 3.1 | Macroscopic Evaluations

During the operations, QSM/nHAp scaffolds were inserted in the cavity at the left side of the mandibula and wetted with host blood. Macroscopically, it was observed that QSM/nHAp scaffolds swelled with host blood and filled the defect cavity even after the first implantation and maintained their structural integrity ten days after the operation (Figure 2). On the other hand, a fibrotic tissue accumulation was detected in all control groups on day 10. At 21st, 45th, and 90th days, the defect surface was covered with thin bone tissue in the control groups. Moreover, during the sample extraction process using a trephine bur, it was observed that the defect area was macroscopically filled with fibrotic and adipose tissue under the superficial thin layer of newly formed bone

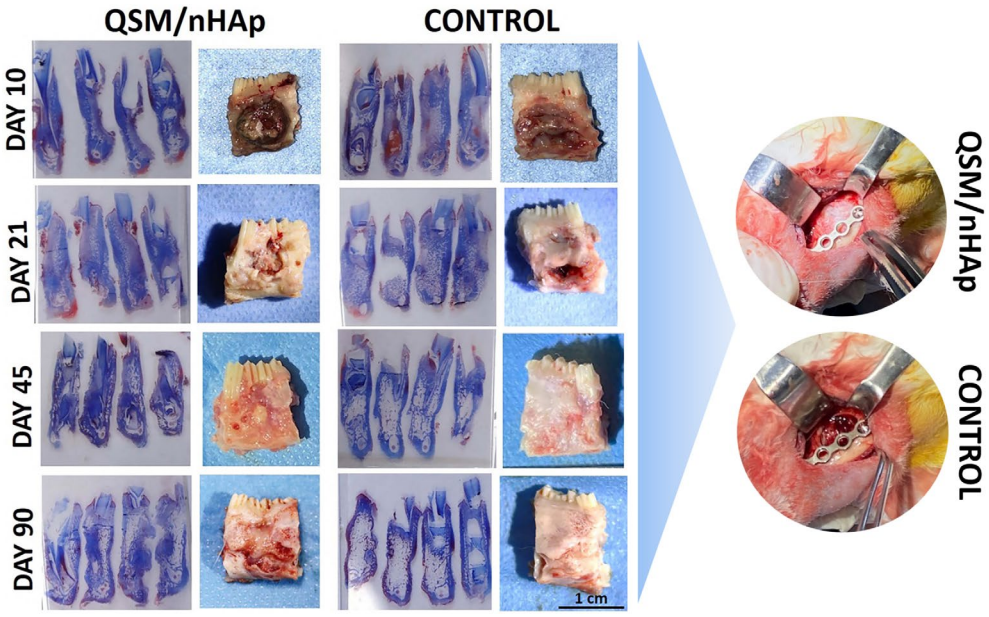


**FIGURE 2** | The macroscopic images of the operated areas with mini-plate fixation at QSM/nHAp implanted and the control side at day 0, and the excised tissue samples with their Masson's trichrome stained specimens at days 10, 21, 45, and 90 control time points (*Scale bar = 1 cm*).

tissue at time points in the healing process. In the QSM/nHAp group, the defect surface was more irregular on day 21st but had a similar macroscopic appearance on days 45th and 90th.

### 3.2 | Histological Observations

To evaluate tissue response over QSM/nHAp scaffolds and analyze the bone-scaffold interface with tissue regeneration within the critically defected area, histochemical (HC) and IHC staining were conducted. HC staining was performed on collected specimens ($n=6$) from rabbit mandibles at days 10, 21, 45, and 90 using H&E, MT, and AR staining (Figure S1). The regeneration of the defective area was followed by IHC staining, where OPN, OSC, and OSN antibodies were applied (Figure S1). On day 10, although there was a moderate inflammatory response in the defect area, no severe immune reaction or biomaterial resorption was observed in the experimental group. While the scaffold-host tissue boundary was visible on day 10, the scaffold was invaded by host cells. The defect area was filled with fibrotic connective tissue in the control group. On day 21, the biomaterial prevented fibrotic tissue migration and gradually resorbed at the base of the defect in the experimental group. However, new bone tissue began to form instead. Meanwhile, fibrotic tissue accumulation was observed in the control group, as seen from HC images. The boundary between the defected area and healthy tissue appeared blurry in the QSM/nHAp group on day 21; this can be attributed to the resorption of the scaffold structure within the host tissue. On day 45, QSM/nHAp was almost totally resorbed in the grafted group, and denser new bone was observed beneath the trabecular bone, accompanied by a small amount of adipose tissue deposition. On the other hand, the control group revealed a lower amount of new bone formation, and the presence of more adipose tissue was greater than that of the QSM/nHAp group. At day 90, both groups revealed a fully recovered morphology over the defected area, which mainly consisted of bone and adipose tissue; however, the ECM expression in terms of calcium deposition and connective tissue accumulation was observed to be greater in QSM/nHAp groups in general (Figure S1).

The scoring table followed a statistical examination of defect healing in Table 1. According to the analyses, all samples have a significant difference ($p<0.01$) within groups at all time points. There was no significant difference within the QSM/nHAp and control groups ($p=1.00$) on days 10 and 90. On the other hand, for days 21 and 45, the bone regeneration pattern was significantly better in the QSM/nHAp groups than in the control groups ($p<0.05$).

According to the IHC staining results, OPN, an ECM protein that regulates bone remodeling and osteoclast adhesion [34], was weakly expressed on days 10 and 21 over the defective zone in both groups. In contrast, the surrounding tissue for both groups exhibited strong OPN expression during the first ten days after the operation. The expression of OPN gradually decreased from day 10 to day 21 and remained at almost the same level after day 45 for both groups. OSC, a non-collagenous protein of bone matrix secreted by mature osteoblast cells [35], revealed a gradual increase from the boundary to the inner side of the defect area from day 10 to day 90. Besides, the expression levels were slightly greater in general QSM/nHAp grafted groups (Figure S1). OSN has a similar expression pattern with OSC till day 45, which indicates the regulation of bone matrix organization and calcium binding in mineralized bone tissue [36]. In general, OPN expression within the defect area was more significant in the control group compared with the QSM/nHAp at day 10. However, for the QSM/nHAp group, the OPN expression was mainly detected over the border of scaffold material (Figure S1). On days 21 and 45, the OPN expression gradually weakened for both groups. On the other hand, at day 90, the OPN expression increased again around newly formed dentine and pulp tissues. OSC expression rate over the operated area significantly improved from day 10 to day 90, and it was observed around the pulp and dentine tissue. OSN expression patterns were also in line with the OPN for both groups. However, the expression rates were more significant in the QSM/nHAp group at all time points (Figure S1).

Interestingly, dental germination was observed in QSM/nHAp samples beginning from day 21 and continued from day 45 to day 90 (Figure 3). QSM/nHAp scaffolds underwent significant change in 21 days post-grafting. Osteodentin formation was observed in the defect area of the QSM/nHAp group. On the contrary, the control group revealed constant fibrous tissue until day 21. On day 45, significant dental tissue formation was observed in QSM/nHAp samples; even the pulp, dentine, and enamel tissues could be observed within the defect zone beneath the compact bone (Figure 3A). On the other hand, control groups mainly revealed adipose deposition followed by fibrotic tissue. On day 90, the connective tissue in the defect differentiated into bone and adipose tissue in the experimental and control groups. In the experimental groups, new dental germs in the defect area were observed in all subjects on days 21, 45, and 90, while new dental germs were observed in only two subjects in the control group on day 90 (Figure 3B).

### 3.3 | μ-CT Examinations

To distinguish between the QSM/nHAp scaffold and newly formed bone tissue in μ-CT images, the QSM/nHAp was initially imaged alone, and the radiographic density related to the scaffold material

**TABLE 1** | Scoring results of control and QSM/nHAp samples at days 10, 21, 45, and 90.

| Experimental groups | Day 10 median (min–max) | Day 21 median (min–max) | Day 45 median (min–max) | Day 90 median (min–max) | |
|---|---|---|---|---|---|
| Control | 2 (1-2)$^{A}$ | 2 (2-3)$^{AB}$ | 3 (3-4)$^{BC}$ | 5 (4-5)$^{C}$ | $p<\mathbf{0.001}$ |
| QSM/nHAp | 2 (1-2)$^{A}$ | 3 (2-4)$^{A}$ | 4 (4)$^{AB}$ | 5 (4-5)$^{B}$ | $p<\mathbf{0.001}$ |
| | $p=1.00$ | $p=\mathbf{0.046}$ | $p=\mathbf{0.025}$ | $p=1.00$ | |

*Note:* Different superscript letters ($^{A, B, C}$) indicate statistically significant differences in rows. $p < 0.05$ indicates the bold values present in the table.

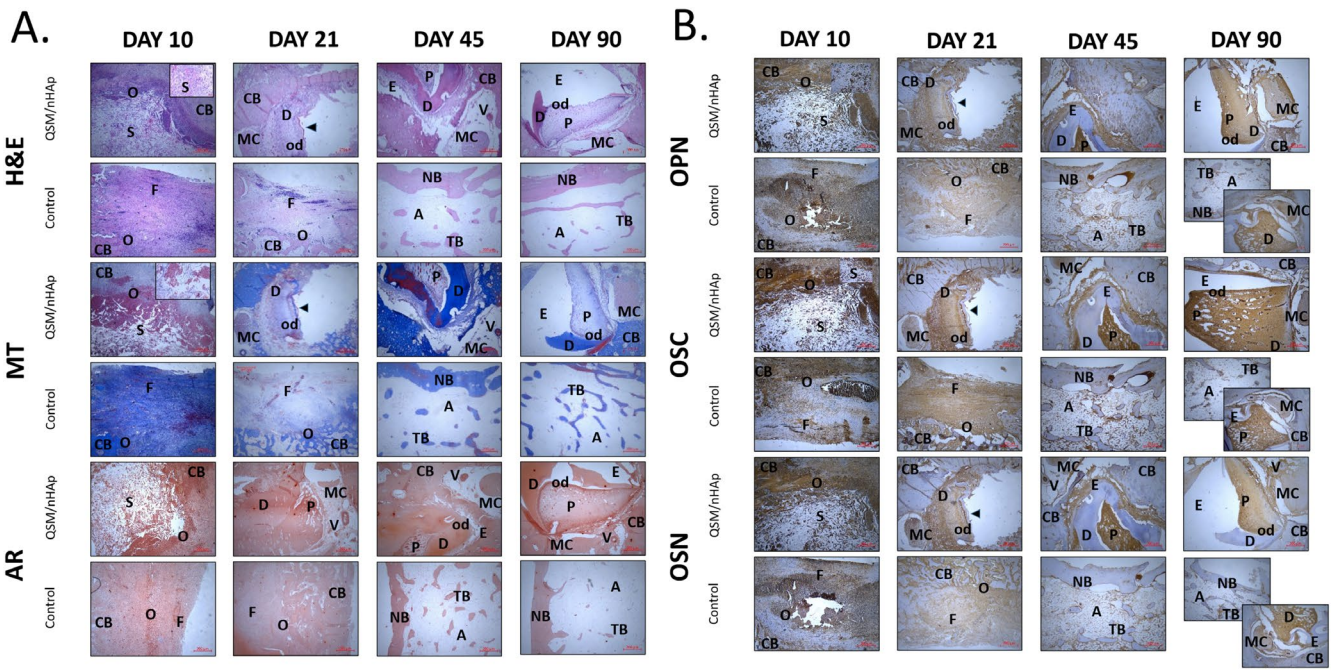


**FIGURE 3** | HC (A) and IHC (B) staining from QSM/nHAp and control samples that show dental regeneration at control points from days 10, 21, 45, and 90. (Histology photomicrographs of Hematoxylin Eosin (H&E), Masson's trichrome staining (MT), Alizarin Red (AR), Osteopontin (OPN), Osteocalcin (OSC), Osteonectin (OSN) 4X; Small rectangle 10X; *scale bar = 200 μm*.) Abbreviations: S, Scaffold; V, Vessels; A, Adipose tissue; F, Collagen fibers; T, Tooth bud; E, Enamel; D, Dentine; od, osteodentin; P, Pulp; TB-Trabecular Bone; O, Osteoblast; CB, Compact Bone; NB, New bone; MC, Mandibular canal; black triangle, the morphogenesis initiation of the tooth.

was noted. The 153 coronal, axial, and sagittal sections of μ-CT images (0.02654 mm voxel size, 10 mm diameter defect area) were independently evaluated. Interestingly, when QSM/nHAp scaffold material was scanned under the same utilized parameters ($kV_p$, mA, and voxel size) as for the samples, the QSM/nHAp scaffold did not produce any radiographic image in μ-CT scans and could not be distinguished radiologically from the surrounding aqueous environment, which is reasonable due to the high water-holding capacity of the scaffold material [22, 23, 25, 27].

The operated area appeared as a gap in the μ-CT images for the QSM/nHAp and control groups on day 10 (Figure 4). On the other hand, on day 21, new bone formation was evident in both groups, and the cavity was nearly filled with new bone density. Strikingly, tooth germs were detected predominantly closer to the base of the defect area in all QSM/nHAp samples, in addition to new bone formation. In contrast, no tooth germ was observed in the control group. On day 45, the experimental group exhibited a clear trabecular structure and distinct tooth germ forms, while the control group revealed a distinct trabecular bone structure. The control and experimental groups displayed regular and substantial bone formation on day 90. Notably, tooth germs were observed closer to the center of the defect in the QSM/nHAp group, while tooth formation was only noted in two samples in the control group on day 90 (Figure 4).

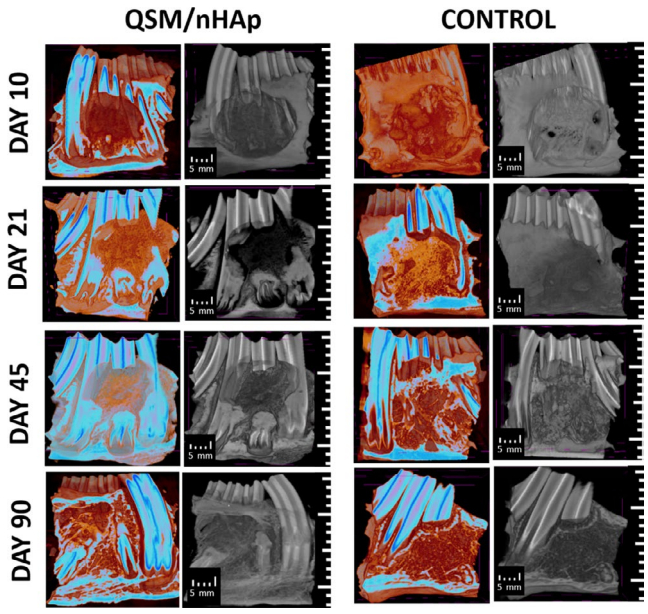


**FIGURE 4** | μ-CT images of QSM/nHAp and control samples at days 10, 21, 45, and 90 (*scale bar = 5 mm*) (blue: high-density mineralized tissue, red: adipose or fibrotic tissue in the defect area or trabecular bone).

## 3.4 | Gene Expressions

The results of the gene expression study conducted with tissues explanted on control time points, following implantations, are presented in Figure 5. Considering the cavity on the left side of the rabbit's mandible was implanted with QSM/nHAp, while the right side was left empty and used as the control group, and this methodology was repeated for samples at each checkpoint date, the gene expression levels were compared separately at given dates with the control groups. When the expression of RunX2, a marker for early osteogenic differentiation, was examined, there was an approximately 2-fold increase in gene

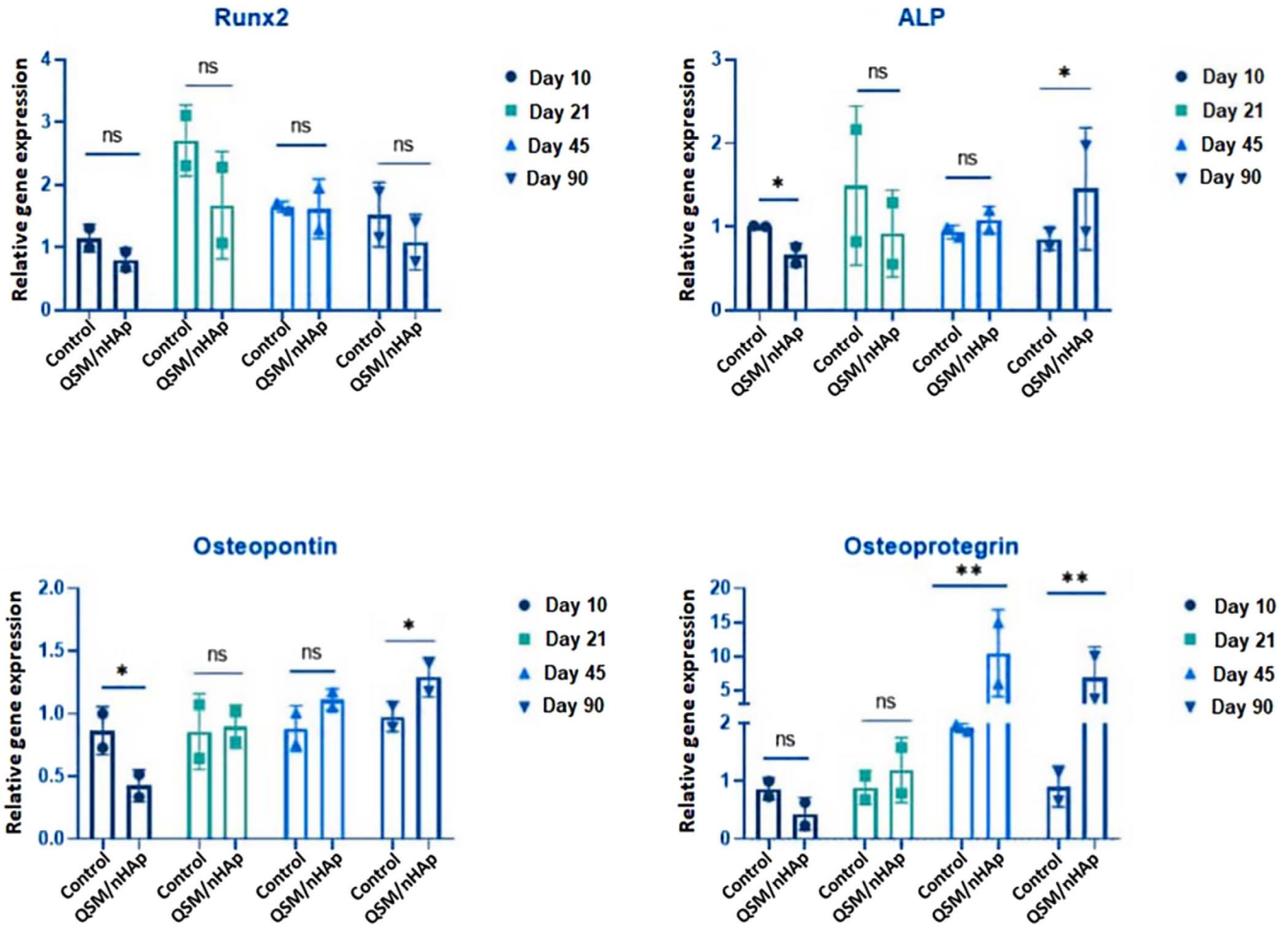


**FIGURE 5** | The qRT-PCR results of cells within QSM/nHAp and control groups at time points day 10, 21, 45, and 90 for Runx transcription factor 2 (RunX2), alkaline phosphatase (ALP), osteopontin and osteoprotegerin markers (ns: non-significant change, *: $p < 0.05$, **: $p < 0.01$).

expression in the QSM/nHAp group on day 21 compared with day 10. This increase in RunX2 expression remained stable in the following time points, which is rational considering the involvement of this gene in early osteogenic differentiation. However, there was no significant difference between the control and experimental groups at any time point. The expression of ALP remained stable in the QSM/nHAp group until day 45. However, there was an approximately 3-fold increase on day 90 compared with day 10, and there was also a statistically significant difference ($p < 0.05$) between the control and experimental groups on day 90. The OPN expression also revealed a gradual increment throughout the post-implantation period. This increase was approximately 3-fold higher in the QSM/nHAp group on day 90 compared with day 10 with a significant difference ($p < 0.05$). Finally, when the expression of OPG, another marker for mature bone tissue, was examined, gene expression was observed during the post-implantation period. This increase was approximately 10-fold higher in the QSM/nHAp group at day 90 than on day 10 ($p < 0.01$).

### 3.5 | SEM Imaging

Figure 6 shows the SEM images of QSM/nHAp and control group samples. As seen from the images, on day 10, both groups revealed a rough morphology with cell infiltration from surrounding tissue. The critically sized cavity is filled with fibrous ECM and cellular structures at the following time points. While the accumulation of fibers is quite visible in the control group, QSM/nHAp displayed a relatively more compact structure on days 21 and 45. On the other hand, the QSM/nHAp group had a more fibrous structure than the control group by day 90. Both groups filled the critically sized hole with newly formed bone tissue.

In line with μ-CT and histological analyses, dental regeneration was observed in QSM/nHAp samples, concurrent with bone regeneration (Figure 7). Accumulation of cylindrical dentinal tubes and the formation of dentin structure were quite visible at day 90, as seen from the SEM images. The ordered position of open tubules over the dentine structure revealed a healthy dental recovery within the QSM/nHAp scaffolds.

## 4 | Discussion

Herein, QSM was enhanced with nHAp to create a QSM/nHAp hybrid scaffold for mandibular bone regeneration. This novel combination, used in vivo for the first time, aimed to improve the osteogenic properties of the scaffold, allowing

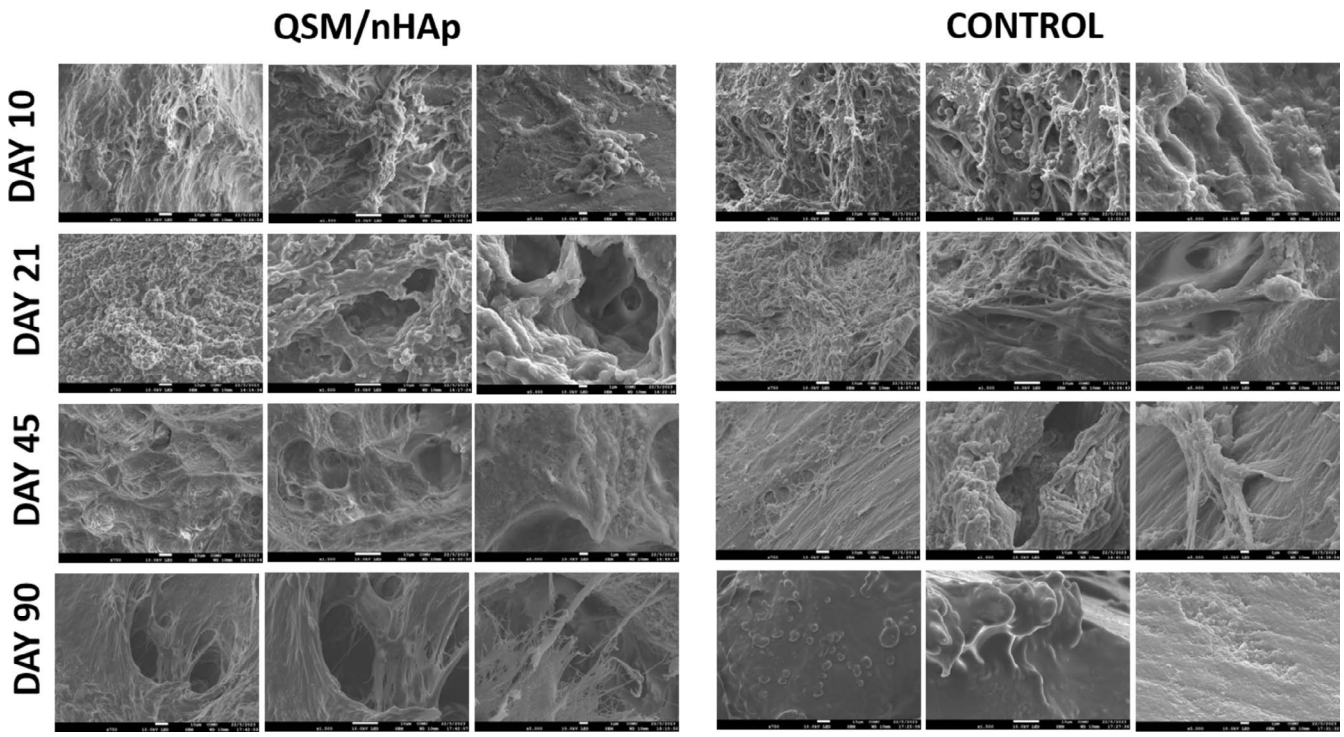


**FIGURE 6** | SEM images of QSM/nHAp and control specimens under different magnifications (750, 1500, and 5000X) at time points day 10, 21, 45, and 90 (*scale bar = 10 μm* for 750 and 1500X, and *Scale bar = 1 μm* for 5000X magnifications).

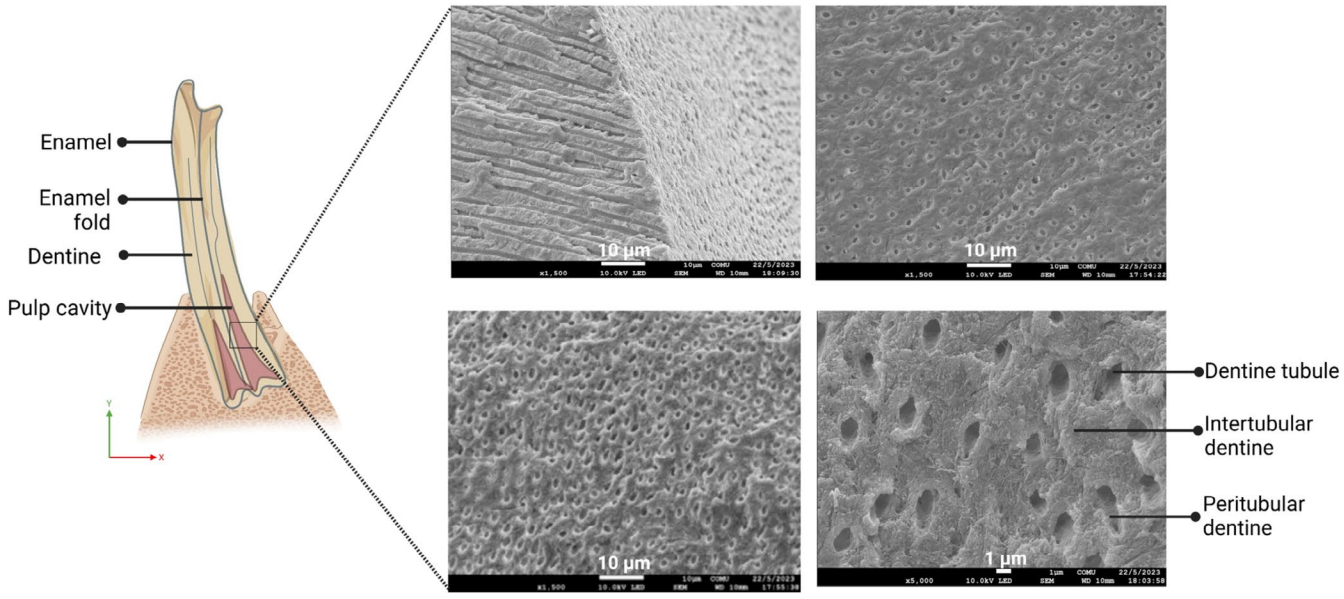


**FIGURE 7** | Structural illustration for rabbit dental tissue (created in BioRender.com) and SEM images taken from day 90 on QSM/nHAp samples that reveal dentine formation (*scale bar = 10 and 1 μm* for 5000X magnification).

it to address critically sized mandibular defects in rabbits effectively. In this way, the regenerative potential of the QSM/nHAp scaffold was translated into the regeneration of critically sized defects to induce proper healing. According to the results, the QSM/nHAp scaffolds successfully supported the bone regeneration together with the co-development of dental germination in vivo. These surprising findings urged the researchers to compare QSM/nHAp performance to existing composite materials.

In the literature, various applied composite scaffold methodologies are valid for in vivo mandibular regeneration in rabbits as a model organism for the evaluation of scaffold bioactivity [2, 6, 11, 37–41]. The combination of hydroxyapatite and polyamide [6, 11], vascular endothelial cells (ECs), and MSCs either on a culture plate or a polylactide glycolic acid (PLGA) scaffold [42], polycaprolactone (PCL) with tricalcium phosphate (TCP) [39], or polycaprolactone/hydroxyapatite/beta calcium phosphate [41] are bioengineered scaffolds for bone defect regeneration.

Among them, Guo et al. developed a hybrid scaffold composed of polyamide and nHAp particles to support bone regeneration and evaluated its efficacy in a rabbit mandibular bone model. They compared the regenerative capacity of the scaffold with three groups: a control (no scaffold), a bare scaffold, and a scaffold with added MSCs. After 28 days, the nHAp-containing scaffolds demonstrated improved bone regeneration compared with the control group. However, no significant differences were observed between the scaffolds with stem cells and those without. Additionally, polyamide residues persisted even after 84 days [6]. Similarly, another group developed a hybrid scaffold using PCL and TCP, testing its bioactivity in mandibular bone defects by comparing control, PCL/TCP, PCL/TCP with cells, and autologous bone grafts. After 4 weeks, the hybrid scaffolds exhibited less bone formation compared with autologous grafts, with no significant differences between cell-containing and bare scaffolds. However, after 8 weeks of implantation, the scaffolds reportedly supported bone regeneration comparable to autologous grafts [38]. In addition to the studies in the literature, research on gelatin and xenogeneic bone powder products such as Gelfoam and Bio-Oss, which are commercially developed and frequently used in bone regeneration, reveals that these products support mandibular bone regeneration and exhibit high biocompatibility [43, 44]. However, since they are of animal origin, they carry a risk of pathogen contamination in clinical applications. Furthermore, it has been observed that Gelfoam, which resorbs very quickly after implantation, is effective only for hemostatic applications and does not fully provide the mechanical support needed for bone regeneration. Similarly, Bio-Oss, available in powder and rigid form, is known not to elastically fill bone cavities and can be hard to implant in complex bone regions anatomically [44].

According to the literature, synthetic polymers, minerals, and their hybrids typically exhibit greater stiffness and mechanical durability than the plant-based QSM/nHAp scaffold presented in this study. However, when considering cellular integrity, biocompatibility, and easy handling in clinical practice, it is hypothesized that plant-based scaffolds provide a better balance of bioactivity and functionality in vivo integration. Besides, even successful results for bone regeneration have been reported in the aforementioned studies; to the best of our knowledge, none of them have demonstrated the co-development of dental and bone regeneration [2]. Therefore, the study conducted with QSM/nHAp is considered valuable and novel with its outstanding ability to serve as a proper niche for bone and dental regeneration simultaneously by being plant-based, economical, and biosafe.

By the end of this study, a positive effect on long-term bone tissue formation at the defect area was observed. Interestingly, compared with that at 45 days, the amount of bone repair at 90 days was slightly lower in the control group. This might be due to the osteoclastic activity of cells within the cavity. The newly formed bone tissue at 45 days in the non-grafted defect cavity may have been resorbed after 90 days. Similar results were also valid in the Campillo et al. study [45]. Strikingly, tooth germination was observed on day 21 within QSM/nHAp scaffolds, while no dental germ was observed in control groups until day 90. The presence of tooth germ was significantly higher in defects implanted with QSM/nHAp than in empty defects. In contrast, no germ formation was observed in control groups, or at the earliest, germ formation began on day 90. These findings were in line with the HC and IHC staining as well. For example, the expression of OPN and OSC, the proteins mainly located in bone and dentine tissue, was quite evident in all QSM/nHAp groups. qRT-PCR results showed upregulation of RunX2, an early osteogenic differentiation marker, in initial implantation stages, while markers for mature bone tissue, including ALP, OPN, and OPG, were upregulated in later stages with significant differences from the control group [46]. The SEM images confirmed the concurrent development of bone and dental tissue within QSM/nHAp scaffolds, aligning with the natural regeneration processes of these tissues [4, 46, 47].

It would be rather ambitious to claim that the developed biomaterial generates new tooth germs. However, it is a fact that the application of QSM/nHAp to the defect site resulted in tooth germ development. This observation implies the QSM/nHAp biomaterial exhibited a proper micro niche by its nHAp-containing hydrophilic environment, which might be leading to the formation of cellular aggregates and the adoption of a spherical morphology [22, 24, 26, 29]. For the osteogenic development, the nHAp content might stimulate bone development by releasing $Ca^{2+}$ ions and triggering the intracellular signaling pathways related to osteogenesis by sustaining a biomimetic environment. On the other hand, the dental development phenomenon can be explained by the hydrophilic nature of the QSM/nHAp hybrid material, which allowed dental progenitor cells to agglomerate within the scaffold, forming spheroid-like structures and potentially triggering dental root formation (Figure S2) along with the continuously growing nature of rabbit teeth [3, 48]. Rabbits have open roots, so the dental regeneration process in normal conditions is relatively rapid, and it is assumed that many stem cells are in the apical parts of the roots. However, all rabbit teeth are hypsodont, which means the tooth has no true root but a long crown structure [48]. Therefore, in this study, the defects were created using a trephine bur, and all related roots were removed from the mandibula; so, no visible dental tissue remained within the cavity in practice after the operation.

In terms of cellular aggregation and differentiation at the damaged side, a previous in vitro study by our group proved that the stem cells were prone to form spheroid structures within the QSM/nHAp scaffold and then differentiated into bone-related cells due to the existence of nHAp particles and the 3D environment of QSM [22]. Similar behavior kinetics might be valid for this in vivo study. According to the performed analyses, it is believed that the natural fibrillation process with mild adipose tissue accumulation inside the QSM/nHAp scaffold might create a proper environment for the aggregation of dental progenitor cells and trigger the tooth organogenesis. Additionally, the composite formulation of the QSM/nHAp biomaterial makes the scaffold flexible in practice. This feature distinguishes nHAp-containing grafts from others in the field by preventing fractures and loss of structural integrity that is commonly seen in bone grafts used clinically. The flexibility of QSH maintains the existing porosity of the scaffold, and it holds the shape while implanting in the defect area. The hydrophilic properties of the material swell within the cavity while keeping the cells inside. The anticipated bone and dental regeneration process stages within the QSM/nHAp scaffold are summarized in Figure S2. Remarkably, while examining the scaffold-based applications of this biopolymer in the existing literature, a consistent pattern

emerged in mammalian cells: they exhibited the formation of a structure resembling a spheroid, accompanied by enhanced viability. These repetitive spheroid-forming results show that QSM/nHAp can create an appropriate niche for spontaneous spheroid formation in vivo studies [22, 23, 25, 27, 29].

## 5 | Conclusions

In this in vivo study, a plant-based therapeutic polymer QSM was enriched with nHAp and utilized as a composite scaffold for mandibular regeneration in rabbits. The porous QSM/nHAp scaffolds absorbed host blood and supported cellular infiltration while revealing a gradual biodegradation profile that facilitated bone regeneration in critical-sized cavities by releasing nHAp particles. A surprising co-development of bone and dental regeneration was observed in QSM/nHAp groups. The hydrophilic, flexible, porous, and durable characteristics of QSM-nHAp scaffolds make a promising option for non–load-bearing applications, particularly in craniomaxillofacial remodeling. Translating this plant-based material from laboratory research to clinical practice is crucial; however, in-depth research is required to understand the intracellular mechanisms underlying dental and bone regenerations with further studies.

### Author Contributions

**Cigdem Cetin Genc:** conceptualization, data curation, formal analysis, funding acquisition, investigation, methodology, project administration, visualization, writing – original draft, writing – review and editing. **Hilal Deniz Yılmaz-Dagdeviren:** data curation, formal analysis, investigation, methodology, writing – original draft. **Yesim Deniz:** data curation, formal analysis, investigation, visualization. **Burak Derkus:** data curation, formal analysis, investigation. **Alpin Degirmenci:** investigation. **Yavuz Emre Arslan:** conceptualization, data curation, formal analysis, investigation, methodology, supervision, writing – original draft, writing – review and editing.

### Acknowledgments

The authors gratefully acknowledge the financial support from Çanakkale Onsekiz Mart University Scientific Research Projects Coordination Unit (Project ID: TSA-2022-4022) and for the use of facilities of the Canakkale Onsekiz Mart University's Science and Technology Application & Research Center (COBILTUM). The authors would also like to thank Mr. Yücel Okatali at MER-TER (Medical, Eskisehir, Türkiye) for his role in the histochemical staining work. They also acknowledge the dedicated efforts of the undergraduate students from the Faculty of Dentistry at Çanakkale Onsekiz Mart University and express appreciation to UMG Uysal Medikal for their support.

### Conflicts of Interest

The authors declare no conflicts of interest.

### Data Availability Statement

The data that support the findings of this study are available from the corresponding authors upon request.

### References

1. A. Nauth, E. Schemitsch, B. Norris, Z. Nollin, and J. T. Watson, "Critical-Size Bone Defects: Is There a Consensus for Diagnosis and Treatment?," *Journal of Orthopaedic Trauma* 32, no. 3 (2018): S7–S11, https://doi.org/10.1097/BOT.0000000000001115.

2. S. Dalfino, P. Savadori, M. Piazzoni, et al., "Regeneration of Critical-Sized Mandibular Defects Using 3D-Printed Composite Scaffolds: A Quantitative Evaluation of New Bone Formation in in Vivo Studies," *Advanced Healthcare Materials* 12, no. 21 (2023): 1–20, https://doi.org/10.1002/adhm.202300128.

3. M. Olaru, L. Sachelarie, and G. Calin, "Hard Dental Tissues Regeneration—Approaches and Challenges," *Materials* 14, no. 10 (2021): 2558, https://doi.org/10.3390/ma14102558.

4. E. Tafazoli Moghadam, M. Yazdanian, M. Alam, et al., "Current Natural Bioactive Materials in Bone and Tooth Regeneration in Dentistry: A Comprehensive Overview," *Journal of Materials Research and Technology* 13 (2021): 2078–2114, https://doi.org/10.1016/j.jmrt.2021.05.089.

5. F. Donnaloja, E. Jacchetti, M. Soncini, and M. T. Raimondi, "Natural and Synthetic Polymers for Bone Scaffolds Optimization," *Polymers* 12, no. 4 (2020): 905, https://doi.org/10.3390/polym12040905.

6. J. Guo, Z. Meng, G. Chen, et al., "Restoration of Critical-Size Defects in the Rabbit Mandible Using Porous Nanohydroxyapatite-Polyamide Scaffolds," *Tissue Engineering Part A* 18, no. 11–12 (2012): 1239–1252, https://doi.org/10.1089/ten.tea.2011.0503.

7. S. J. Jang, S. E. Kim, T. S. Han, J. S. Son, S. S. Kang, and S. H. Choi, "Bone Regeneration of Hydroxyapatite With Granular Form or Porous Scaffold in Canine Alveolar Sockets," *In Vivo* 31, no. 3 (2017): 335–341.

8. W. Liang, P. Ding, G. Li, E. Lu, and Z. Zhao, "Hydroxyapatite Nanoparticles Facilitate Osteoblast Differentiation and Bone Formation Within Sagittal Suture During Expansion in Rats," *Drug Design, Development and Therapy* 15 (2021): 905–917, https://doi.org/10.2147/DDDT.S299641.

9. S. Von Euw, Y. Wang, G. Laurent, et al., "Bone Mineral: New Insights Into Its Chemical Composition," *Scientific Reports* 9, no. 1 (2019): 1–11, https://doi.org/10.1038/s41598-019-44620-6.

10. H. Shi, Z. Zhou, W. Li, Y. Fan, Z. Li, and J. Wei, "Hydroxyapatite Based Materials for Bone Tissue Engineering: A Brief and Comprehensive Introduction," *Crystals* 11, no. 2 (2021): 1–18, https://doi.org/10.3390/cryst11020149.

11. J. C. Zhang, H. Y. Lu, G. Y. Lv, A. C. Mo, Y. G. Yan, and C. Huang, "The Repair of Critical-Size Defects With Porous Hydroxyapatite/Polyamide Nanocomposite: An Experimental Study in Rabbit Mandibles," *International Journal of Oral and Maxillofacial Surgery* 39, no. 5 (2010): 469–477, https://doi.org/10.1016/j.ijom.2010.01.013.

12. Y. Zhu, N. Cao, Y. Zhang, et al., "The Ability and Mechanism of nHAC/CGF in Promoting Osteogenesis and Repairing Mandibular Defects," *Nanomaterials* 12, no. 2 (2022): 1–16, https://doi.org/10.3390/nano12020212.

13. G. Radha, N. Manjubaashini, and S. Balakumar, "Nano-Hydroxyapatite/Natural Polymer Composite Scaffolds for Bone Tissue Engineering: A Brief Review of Recent Trend," *In vitro models* 2, no. 5 (2023): 125–151, https://doi.org/10.1007/s44164-023-00049-w.

14. G. Wei and P. X. Ma, "Structure and Properties of Nano-Hydroxyapatite/Polymer Composite Scaffolds for Bone Tissue Engineering," *Biomaterials* 25, no. 19 (2004): 4749–4757, https://doi.org/10.1016/j.biomaterials.2003.12.005.

15. A. Indurkar, A. Pandit, R. Jain, and P. Dandekar, "Plant-Based Biomaterials in Tissue Engineering," *Bioprinting* 21, no. December 2020 (2021): e00127, https://doi.org/10.1016/j.bprint.2020.e00127.

16. S. Iravani and R. S. Varma, "Plants and Plant-Based Polymers as Scaffolds for Tissue Engineering," *Green Chemistry* 21, no. 18 (2019): 4839–4867, https://doi.org/10.1039/c9gc02391g.

17. R. Mohanraj, "Plant-Derived Resorbable Polymers in Tissue Engineering," in *Materials for Biomedical Engineering: Absorbable Polymers*,

ed. I. Elsevier (Elsevier Inc, 2019), https://doi.org/10.1016/B978-0-12-818415-8.00002-4.

18. M. A. Hussain, G. Muhammad, M. T. Haseeb, and M. N. Tahir, "Quince Seed Mucilage: A Stimuli-Responsive/Smart Biopolymer," in *Functional Biopolymers. Polymers and Polymeric Composites: A Reference Series*, eds. M. Jafar Mazumder, H. Sheardown, and A. Al-Ahmed (Springer, 2019), 127–148, https://doi.org/10.1007/978-3-319-95990-0_19.

19. M. Jouki, F. T. Yazdi, S. A. Mortazavi, and A. Koocheki, "Quince Seed Mucilage Films Incorporated With Oregano Essential Oil: Physical, Thermal, Barrier, Antioxidant and Antibacterial Properties," *Food Hydrocolloids* 36 (2014): 9–19, https://doi.org/10.1016/j.foodhyd.2013.08.030.

20. S. Sabir, R. Qureshi, M. Arshad, et al., "Pharmacognostic and Clinical Aspects of *Cydonia Oblonga*: A Review," *Asian Pacific Journal of Tropical Disease* 5, no. 11 (2015): 850–855, https://doi.org/10.1016/S2222-1808(15)60934-3.

21. P. Tamri, A. Hemmati, and M. G. Boroujerdnia, "Wound Healing Properties of Quince Seed Mucilage: In Vivo Evaluation in Rabbit Full-Thickness Wound Model," *International Journal of Surgery* 12, no. 8 (2014): 843–847, https://doi.org/10.1016/j.ijsu.2014.06.016.

22. C. Cetin Genc, H. D. Yilmaz, B. Karaca, F. Kiran, and Y. E. Arslan, "Nano-Hydroxyapatite Incorporated Quince Seed Mucilage Bioscaffolds for Osteogenic Differentiation of Human Adipose-Derived Mesenchymal Stem Cells," *International Journal of Biological Macromolecules* 195 (2022): 492–505, https://doi.org/10.1016/j.ijbiomac.2021.12.054.

23. M. Guzelgulgen, D. Ozkendir-Inanc, U. H. Yildiz, and A. Arslan-Yildiz, "Glucuronoxylan-Based Quince Seed Hydrogel: A Promising Scaffold for Tissue Engineering Applications," *International Journal of Biological Macromolecules* 180 (2021): 729–738, https://doi.org/10.1016/j.ijbiomac.2021.03.096.

24. A. Izadyari Aghmiuni, S. Heidari Keshel, F. Sefat, and A. Akbarzadeh Khiyavi, "Quince Seed Mucilage-Based Scaffold as a Smart Biological Substrate to Mimic Mechanobiological Behavior of Skin and Promote Fibroblasts Proliferation and h-ASCs Differentiation Into Keratinocytes," *International Journal of Biological Macromolecules* 142 (2020): 668–679, https://doi.org/10.1016/j.ijbiomac.2019.10.008.

25. E. Şimşek, B. Karaca, and Y. E. Arslan, "Bioengineered Three-Dimensional Physical Constructs From Quince Seed Mucilage for Human Adipose-Derived Mesenchymal Stem Cells," *Journal of Bioactive and Compatible Polymers* 35, no. 3 (2020): 240–253, https://doi.org/10.1177/0883911520918390.

26. Ö. Yildirim and A. Arslan-Yildiz, "Development of a Hydrocolloid Bio-Ink for 3D Bioprinting," *Biomaterials Science* 10, no. 23 (2022): 6707–6717, https://doi.org/10.1039/D2BM01184K.

27. H. D. Yilmaz, U. Cengiz, Y. E. Arslan, F. Kiran, and A. Ceylan, "From a Plant Secretion to the Promising Bone Grafts: Cryogels of Silicon-Integrated Quince Seed Mucilage by Microwave-Assisted Sol–Gel Reaction," *Journal of Bioscience and Bioengineering* 131, no. 4 (2021): 420–433, https://doi.org/10.1016/j.jbiosc.2020.11.008.

28. A. ChuRoqia, S. Hasham, M. A. B. Sofi, S. A. Shafquat Majeed, and F. A. Sheikh, *Novel Biomaterials for Regenerative Medicine/ Prospects of Natural Polymeric Scaffolds in Peripheral Nerve Tissue-Regeneration (p. 533)* (Springer, 2018).

29. H. D. Yilmaz, U. Cengiz, B. Derkus, and Y. E. Arslan, "Development of Plant-Based Biopolymer Coatings for 3D Cell Culture: Boron-Silica-Enriched Quince Seed Mucilage Nanocomposites," *Biomaterials Science* 11, no. 15 (2023): 5320–5336, https://doi.org/10.1039/d3bm00170a.

30. Guidelines, A, "The ARRIVE Guidelines 2.0," n.d.

31. N. Percie du Sert, A. Ahluwalia, S. Alam, et al., "Reporting Animal Research: Explanation and Elaboration for the ARRIVE Guidelines 2.0," *PLoS Biology* 18, no. 7 (2020): e3000411, https://doi.org/10.1371/journal.pbio.3000411.

32. M. F. W. F. D. G. Altman, "Guidelines for the Design and Statistical Analysis of Experiments Using Laboratory Animals," *ILAR Journal* 43, no. 4 (2002): 244–258.

33. M. H. Huo, N. W. Troiano, R. R. Pelker, C. M. Gundberg, and G. E. Friedlaender, "The Influence of Ibuprofen on Fracture Repair: Biomechanical, Biochemical, Histologic, and Histomorphometric Parameters in Rats," *Journal of Orthopaedic Research* 9, no. 3 (1991): 383–390, https://doi.org/10.1002/jor.1100090310.

34. A. O'Regan and J. S. Berman, "Osteopontin: A Key Cytokine in Cell-Mediated and Granulomatous Inflammation," *International Journal of Experimental Pathology* 81, no. 6 (2000): 373–390, https://doi.org/10.1046/j.1365-2613.2000.00163.x.

35. R. S. Dradjat, P. Sananta, R. D. Rosandi, and L. D. Siahaan, "Osteocalcin Biomarker Level Evaluation on Fracture Healing With Bone Defect After Stromal Vascular Fraction Application in Murine Model," *Annals of Medicine and Surgery* 71, no. October (2021): 103020, https://doi.org/10.1016/j.amsu.2021.103020.

36. G. Calabrese, R. Giuffrida, S. Forte, et al., "Bone Augmentation After Ectopic Implantation of a Cell-Free Collagen-Hydroxyapatite Scaffold in the Mouse," *Scientific Reports* 6, no. 1 (2016): 36399, https://doi.org/10.1038/srep36399.

37. C. Kim, H. J. Yang, T. H. Cho, et al., "Implantable Electrical Stimulation Bioreactor With Liquid Crystal Polymer-Based Electrodes for Enhanced Bone Regeneration at Mandibular Large Defects in Rabbit," *Medical and Biological Engineering and Computing* 58, no. 2 (2020): 383–399, https://doi.org/10.1007/s11517-019-02046-2.

38. S. Kotagudda Ranganath, M. Schlund, J. Delattre, J. Ferri, and F. Chai, "Bilateral Double Site (Calvarial and Mandibular) Critical-Size Bone Defect Model in Rabbits for Evaluation of a Craniofacial Tissue Engineering Constructs," *Materials Today Bio* 14, no. April (2022): 100267, https://doi.org/10.1016/j.mtbio.2022.100267.

39. T. Nuntanaranont, T. Promboot, and S. Sutapreyasri, "Effect of Expanded Bone Marrow-Derived Osteoprogenitor Cells Seeded Into Polycaprolactone/Tricalcium Phosphate Scaffolds in New Bone Regeneration of Rabbit Mandibular Defects," *Journal of Materials Science: Materials in Medicine* 29, no. 3 (2018): 24, https://doi.org/10.1007/s10856-018-6030-z.

40. F. Xu, H. Ren, M. Zheng, et al., "Development of Biodegradable Bioactive Glass Ceramics by DLP Printed Containing EPCs/BMSCs for Bone Tissue Engineering of Rabbit Mandible Defects," *Journal of the Mechanical Behavior of Biomedical Materials* 103, no. November 2019 (2020): 103532, https://doi.org/10.1016/j.jmbbm.2019.103532.

41. H. z. Xu and J. s. Su, "Restoration of Critical Defects in the Rabbit Mandible Using Osteoblasts and Vascular Endothelial Cells Co-Cultured With Vascular Stent-Loaded Nano-Composite Scaffolds," *Journal of the Mechanical Behavior of Biomedical Materials* 124, no. February (2021): 104831, https://doi.org/10.1016/j.jmbbm.2021.104831.

42. J. Liu, C. Liu, B. Sun, et al., "Differentiation of Rabbit Bone Mesenchymal Stem Cells Into Endothelial Cells in Vitro and Promotion of Defective Bone Regeneration in Vivo," *Cell Biochemistry and Biophysics* 68, no. 3 (2014): 479–487, https://doi.org/10.1007/s12013-013-9726-1.

43. A. A. Ashour, M. Zaghloul, W. Mahmoud, M. E. Helal, and M. E. Grawish, "Gelfoam Haemostatic Agent With or Without Autologous Bone Marrow-Derived Stem Cells for the Regeneration of Critical-Size Mandibular Defects in the Rabbit," *International Journal of Oral and Maxillofacial Surgery* 47, no. 11 (2018): 1488–1494, https://doi.org/10.1016/j.ijom.2018.04.021.

44. T. Jensen, S. Schou, A. Stavropoulos, H. Terheyden, and P. Holmstrup, "Maxillary Sinus Floor Augmentation With Bio-Oss or Bio-Oss Mixed With Autogenous Bone as Graft: A Systematic Review," *Clinical Oral Implants Research* 23, no. 3 (2012): 263–273, https://doi.org/10.1111/j.1600-0501.2011.02168.x.

45. V.-E. Campillo, S. Langonnet, A. Pierrefeu, and A.-G. Chaux-Bodard, "Anatomic and Histological Study of the Rabbit Mandible as an Experimental Model for Wound Healing and Surgical Therapies," *Laboratory Animals* 48, no. 4 (2014): 273–277, https://doi.org/10.1177/0023677214540635.

46. S. Albeshri, A. Alblaihess, A. A. Niazy, S. Ramalingam, C. Sundar, and H. S. Alghamdi, "Biomarkers as Independent Predictors of Bone Regeneration Around Biomaterials: A Systematic Review of Literature," *Journal of Contemporary Dental Practice* 19, no. 5 (2018): 605–618, https://doi.org/10.5005/jp-journals-10024-2306.

47. C. Morsczeck and G. Schmalz, "Transcriptomes and Proteomes of Dental Follicle Cells," *Journal of Dental Research* 89, no. 5 (2010): 445–456, https://doi.org/10.1177/0022034510366899.

48. Z. H. Ali and R. Mubarak, "Histomorphological Study of Dentine Pulp Complex of Continuously Growing Teeth in the Rabbits," *Life Science Journal* 9, no. 3 (2012): 1554–1564, https://www.lifesciencesite.com/lsj/life0903/226_10287life0903_1554_1564.pdf.

## Supporting Information

Additional supporting information can be found online in the Supporting Information section.